Journal of Engineering Science 13(1), 2022, 97-104
DOI: https://doi.org/10.3329/jes.v13i1.60567

JES
an international Journal

LINEAR AND NONLINEAR SPHERICALLY SYMMETRIC PERTURBATION IN ASTROPHYSICAL COMPACT OBJECTS

Muhammad Asaduzzaman

Department of Physics
Khulna University of Engineering and Technology, Khulna-9203, Bangladesh

Received: 20 December, 2021 Accepted: 25 March2022

ABSTRACT

A degenerate quantum plasma system (DQPS) consisting of arbitrary number of degenerate light (electron, proton, neutron, etc.) and heavy (light nuclei/element, heavy nuclei/element, etc.) particle species is considered to investigate the spherically symmetric perturbation (both linear and nonlinear) of self-gravitational field. The fundamental characteristics (amplitude, width, etc.) of small amplitude self-gravitational potential structures, which are found to be formed in the considered plasma system, are examined by the reductive perturbation technique. The derivation and numerical analysis of the modified Korteweg-de Vries (mKdV) equation are obtained. The analytical results are applied in astrophysical compact objects like white dwarfs and neutron stars, which are the examples of DQPS.

Keywords: *Compact objects, Degenerate pressure, Nonlinearity, Relativity, Self-gravitational perturbation, Solitary waves.*

1. INTRODUCTION

Nowadays, wave phenomena in dense degenerate quantum plasma have received a considerable attention because of its ubiquity in many astrophysical compact objects. As the density of a classical plasma increases, or its temperature decreases, it can enter a regime when the quantum nature of its constituent particles starts to affect its macroscopic properties and dynamics, and such plasmas are then called quantum plasmas. This quantum plasma system which contains degenerate fermions (e.g., electrons) is known as DQPS. The astrophysical compact objects like white dwarfs, neutron stars and black holes are the examples of aforementioned plasmas, where matters exist in extreme conditions (Chandrasekhar, 1931; Chandrasekhar, 1931a; Chandrasekhar, 1935; Garcia-Berro *et al.*, 2010; Koester and Chanmugam, 1990; Shapiro and Teukolsky, 1983).

Many researchers (Brodin and Marklund, 2007; Haas, 2007; Hossen and Mamun, 2015; Hossen and Mamun, 2014; Hossen *et al.*, 2014; Marklund and Brodin, 2007; Marklund *et al.*, 2007; Masood *et al.*, 2010; Manfredi, 2005; Misra and Samanta, 2008; Misra *et al.*, 2010; Shukla and Eliasson, 2006; Shukla and Eliasson, 2007) studied the propagation of electrostatic excitations (in the form of solitary waves, shock structures, double layers, etc.) in a plasma system (which follows the laws of quantum mechanics) by considering only the light particles as the degenerate particle. In our previous paper (Asaduzzaman, 2017) we also considered a plasma system where electron (light particle) was only degenerate. In our present work, we consider a general DQPS consisting of arbitrary number of light particle species s and heavy particle species j in which both light and heavy particle species are degenerate. We want to investigate here the basic characteristics of linear and nonlinear self-gravitational potential structures (SGPS) by assuming a quantum plasma system (highly dense) consisting of non-relativistic degenerate light and heavy particle species.

For a non-relativistic degenerate plasma particle species, the equation of state can be represented by (Chandrasekhar, 1931; Chandrasekhar, 1931a; Chandrasekhar, 1935) $P_i = K_i N_i^{5/3}$, where P_i is the degenerate plasma particle pressure for i-species, N_i is the degenerate plasma particle number density for i-species, K_i is the m_j constant of proportionality, and $i = s, j$ stands for s-species and j–species, respectively. The proportionality constant
K_i is given by

*Corresponding Author: azaman@phy.kuet.ac.bd
ISSN 2075-4914 (print); ISSN 2706-6835 (online)

$$K_i = \frac{3}{5}\left(\frac{\pi}{3}\right)^{1/3}\frac{\pi\hbar^2}{m_i} \simeq \frac{3}{5}L_q\hbar c, \tag{1}$$

where $L_q = \pi\hbar/m_i c$.

The manuscript is coordinated in the following fashion: The governing equations of the assumed plasma model are expressed in Sec. 2. The linear dispersion relation and the mKdV equation are derived in Sec. 3 and 4, respectively. The graphical and numerical observations are presented in Sec. 5. Finally, the summary of our results and discussion are provided in Sec. 6.

2. GOVERNING EQUATIONS

We assume a nonplanar geometry (spherical) and examine the fundamental properties of the SGPS for both linear and nonlinear cases in a quantum plasma system (which is highly dense and degenerate) containing arbitrary number of non-relativistic degenerate light particle species *s* and heavy particle species *j*.
According to Fowler (Fowler, 1994), who has revisited the work of Chandrasekhar (Chandrasekhar, 1931), the pressure balance equation is

$$K_s\frac{\partial N_s^{5/3}}{\partial r} = -m_s N_s\frac{\partial \Psi}{\partial r}. \tag{2}$$

The normalized form of Eq. (2) is

$$\rho_s = \left[1 - \frac{2}{3}\alpha_s\psi\right]^{3/2}. \tag{3}$$

The normalized continuity and momentum balance equations for heavy particle species are given by

$$\frac{\partial \rho_j}{\partial t} + \frac{1}{r^\nu}\frac{\partial}{\partial r}\left(r^\nu \rho_j u_j\right) = 0, \tag{4}$$

$$\frac{\partial u_j}{\partial t} + u_j\frac{\partial u_j}{\partial r} = -\frac{\partial \psi}{\partial r} - \frac{3}{2}\beta_j\frac{\partial \rho_j^{2/3}}{\partial r}. \tag{5}$$

The Poisson's equation for the self-gravitational potential is

$$\frac{1}{r^\nu}\frac{\partial}{\partial r}\left(r^\nu\frac{\partial \psi}{\partial r}\right) = \sum_s \gamma_s(\rho_s - 1) + \sum_j \delta_j(\rho_j - 1), \tag{6}$$

where $\nu = 2$ ($\nu = 0$) for spherical (planar) geometry; $\rho_s(\rho_j)$ is the mass density of the degenerate light(heavy) particle species $s(j)$, and is normalized by the equilibrium mass density $\rho_{s0}(\rho_{j0})$ of the degenerate particle species $s(j)$; $u_j$is the speed of the degenerate fluid of species j, and is normalized by $C_q = \frac{\sqrt{\pi}\,\hbar}{m_c}\left(\frac{\rho_{e0}}{m_e}\right)^{1/3}$in which $m_c(m_e)$ is the rest mass of carbon(electron); ψ is the self-gravitational potential, and is normalized by C_q^2; $\alpha_s = \left(\frac{m_s}{m_c}\right)^2\left(\frac{m_s}{m_e}\right)^{2/3}\left(\frac{\rho_{e0}}{\rho_{s0}}\right)^{2/3}$,$\beta_j = \left(\frac{m_c}{m_j}\right)^2\left(\frac{m_e}{m_j}\right)^{2/3}\left(\frac{\rho_{j0}}{\rho_{e0}}\right)^{2/3}$, in which $m_s(m_j)$ is the mass of the degenerate particle species $s(j)$; $\rho_s = m_s n_s$and $\rho_j = m_j n_j$. The time variable (t) is normalized by the inverse of the carbon Jeans frequency (Jeans, 1929) $\omega_{Jc} = \sqrt{4\pi G\rho_c}$; $r$is the space variable normalized by$L_q = C_q/\omega_{Jc}$; $\gamma_s = \rho_{s0}/\rho_{c0}$, and $\delta_j = \frac{\rho_{j0}}{\rho_{c0}}$.

3. LINEAR DISPERSION RELATION

We assume $\nu = 0$ (one dimensional geometry) to get the linear dispersion relation for the self-gravitational perturbation in which the physics remains unchanged. Linearizing Equations (4) - (6) and assuming that all the perturbed quantities are proportional to $\exp(-i\omega t + ikr)$, where ω is the angular frequency (normalized by ω_{Jc}) and k is the constant of propagation (normalized by L_q^{-1}) of the self-gravitational perturbation mode (SGPM),and carrying-out Fourier transformation, the linear dispersion relation can be written as

$$\sum_j \frac{\frac{\omega^2}{k^2} - \beta_j}{\delta_j} = \frac{1}{\sum_s(\gamma_s\alpha_s - k^2)}. \tag{7}$$

The above equation represents the linear dispersion relation in general form and is applicable for any kind of astrophysical compact object like white dwarfs and neutron stars. For example, if we consider white dwarfs with electrons as the degenerate light particle species (s-species), and $^{12}_{6}C$ and $^{85}_{37}Rb$ as the degenerate heavy particle species (j-species) then the dispersion relation becomes

$$\frac{\omega^2}{k^2} = \left[\frac{1}{\gamma_e\alpha_e - k^2} + \frac{\beta_C\delta_{Rb} + \delta_C\beta_{Rb}}{\delta_C\delta_{Rb}}\right]\frac{\delta_C\delta_{Rb}}{\delta_C + \delta_{Rb}}. \tag{8}$$

Equation (8) consists of both real and imaginary parts.

4. DERIVATION OF mKDV EQUATION

To investigate the nonlinear properties of the SGPM in the plasma system under consideration, we must consider the nonlinear terms in Equations (3) - (6). Therefore, in order to study the nonlinear propagation of this mode, we first introduce the stretched coordinates (Maxon and Viecelli, 1974; Mamun and Shukla, 2002)

$$\xi = \epsilon^{1/2}\left(r - V_p t\right), \tag{9}$$

$$\tau = \epsilon^{3/2} t, \tag{10}$$

Here, V_p represents the phase speed of the wave and ϵ measures the weakness of the amplitude or dispersion ($0 < \epsilon < 1$). Power series expansion of ρ_j, u_j, and ψ becomes

$$\left.\begin{aligned} \rho_j &= 1 + \epsilon\rho_{j1} + \epsilon^2\rho_{j2} + \cdots\cdots, \\ u_j &= \epsilon u_{j1} + \epsilon^2 u_{j2} + \cdots\cdots, \\ \psi &= \epsilon\psi_1 + \epsilon^2\psi_2 + \cdots\cdots. \end{aligned}\right\} \tag{11}$$

With the help of Eq. (11), various equations can be obtained in powers of ϵ. The lowest order in ϵ, Equations (3) - (6) give

$$u_{j1} = \frac{\psi_1 V_p}{(V_p^2 - \beta_j)} \text{ and } \rho_{j1} = \frac{\psi_1}{(V_p^2 - \beta_j)}.$$

If we consider the next higher order for ϵ, we obtain the following equations

$$\frac{\partial\rho_{j1}}{\partial\tau} - V_p\frac{\partial\rho_{j2}}{\partial\xi} + \frac{\partial}{\partial\xi}\left[\rho_{j1}u_{j1} + u_{j2}\right] + \frac{\nu}{V_p\tau}u_{j1} = 0, \tag{12}$$

$$\frac{\partial u_{j1}}{\partial\tau} - V_p\frac{\partial u_{j2}}{\partial\xi} + u_{j1}\frac{\partial u_{j1}}{\partial\xi} + \frac{\partial\psi_2}{\partial\xi} + \beta_j\frac{\partial}{\partial\xi}\left[\rho_{j2} - \frac{\rho_{j1}^2}{6}\right] = 0, \tag{13}$$

and

$$\frac{\partial^2\psi_1}{\partial\xi^2} = -\sum_s\gamma_s\alpha_s\psi_2 + \sum_s\frac{1}{6}\gamma_s\alpha_s^2\psi_1^2 + \sum_j\delta_j\rho_{j2}. \tag{14}$$

Combining Equations (12) - (14), we readily obtain a mKdV type equation (containing negative dispersion coefficient) in the following form

$$\frac{\partial\psi_1}{\partial\tau} + \frac{\nu}{2\tau}\psi_1 + A\psi_1\frac{\partial\psi_1}{\partial\xi} - B\frac{\partial^3\psi_1}{\partial\xi^3} = 0, \tag{15}$$

where

$$A = \frac{3}{2V_p\sum_j\delta_j\alpha_j^2}\left[\sum_j\delta_j\alpha_j^3\left(1 - \frac{\beta_j}{9V_p^2}\right) + \frac{V_p^4}{9}\sum_s\gamma_s\alpha_s^2\right],$$

$B = \sum_j \frac{\left(V_p^2 - \beta_j\right)^2}{2\delta_j V_p}$, and $\alpha_j = \frac{1}{\left(1 - \frac{\beta_j}{V_p^2}\right)}$.

5. GRAPHICAL AND NUMERICAL OBSERVATIONS

From graphical representation of the linear dispersion relation [Equation (8)], it is clear that both stable and unstable regions exist. Here stable region represents real part and unstable region represents imaginary parts. The variations of ω^2 with electron number density $n_{e0}$and wave number k, with carbon number density $n_{c0}$and wave number k, with rubidium number density n_{r0} and wave number k are shown in Figs. 1, 2, and 3 respectively. Real ω versus k and imaginary ω versus k curves are shown in Figures 4 and 5, respectively.

It is clear from Figure 1 that the frequency increases when the number density of electron increases and the position of unstable region shifted as the number density of electron increases. The frequency variation with carbon number density which is displayed in Figure 2 is different from Figure 1. In Figure 2, we see that the position of unstable region depends only on the carbon number density not on the wave number when the carbon number density is very low. The frequency also decreases as the carbon number density increases. Figure 3 shows that the frequency and the position of unstable region remain same as the rubidium number density changes (increases or decreases). Figures 4 and 5 discloses that the frequency of the SGPM increases exponentially with propagation constant (or decreases exponentially with wavelength) and the growth rate (the positive imaginary part of ω) of the SGPM decreases almost exponentially with propagation constant (or increases almost exponentially with wavelength), respectively.

We have already mentioned that ν = 0 indicates planar geometry. The steady state solution of Equation (15) with ν = 0 is obtained by transforming ξ and τ to $\zeta = \xi - u_0\tau$ and $\tau = \tau$, where u_0 is a constant velocity normalized to C_q, and imposing the appropriate boundary conditions, viz., $\psi_1 \to 0, \frac{d\psi_1}{d\zeta} \to 0, \frac{d^2\psi_1}{d\zeta^2} \to 0$ at $\zeta \to \pm\infty$. Thus, we can express the steady state solution of Equation (15) as

$$\psi_1 = \psi_m Sec^2\left[\frac{\zeta}{\Delta}\right], \tag{16}$$

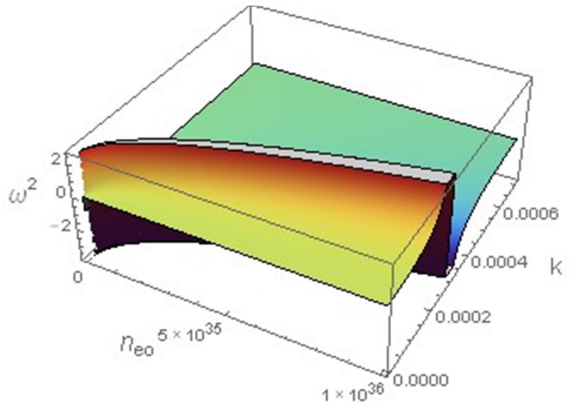

Figure 1: (Color online) Variation of ω^2 with n_{e0}(number density of electron at equilibrium) and k for n_{c0}=10^{30} cm^{-3}, n_{r0}= 10^{30} cm^{-3}, m_c = 12m_p, and m_r= 85m_p($m_p$represents the proton mass).

where $\psi_m = \frac{3u_0}{A}$ is the amplitude and $\Delta = \sqrt{4B/u_0}$ is the width of the SGPS. From Equation (16), it is clear that the self-gravitational potential becomes positive when the velocity u_0>0. We have also observed that as u_0 increases $\psi_m$increases while Δdecreases. The SGPS obtained by solving Eq. (15) numerically is depicted in Figure 6. Figure 6 reveals that the SGPS in the planar geometry are U-shaped structures and are independent of τ.

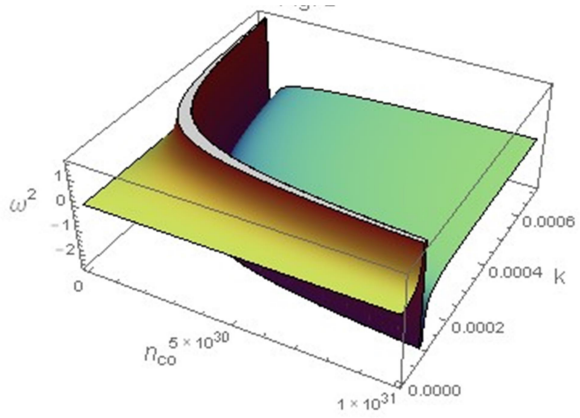

Figure 2: (Color online) Showing the variation of ω^2 with n_{c0} (carbon number density at equilibrium) and k for $n_{e0}= 10^{36}$ cm^{-3}, $n_{r0}= 10^{30}$ cm^{-3}, $m_c= 12m_p$, and $m_r= 85m_p$.

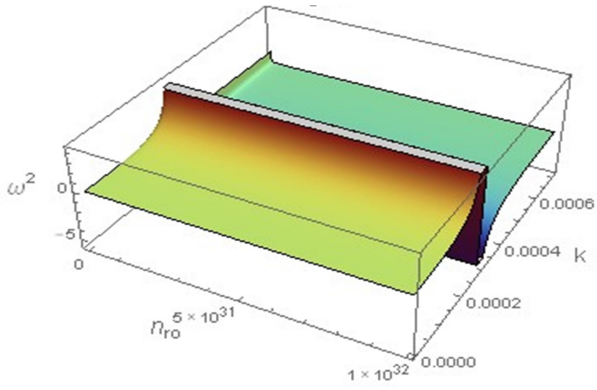

Figure 3: (Color online) Variation of ω^2 with n_{r0}(number density of rubidium at equilibrium) and k for n_{eo}=10^{36} cm^{-3}, $n_{c0}= 10^{30}$ cm^{-3}, $m_c= 12m_p$, and $m_r= 85m_p$.

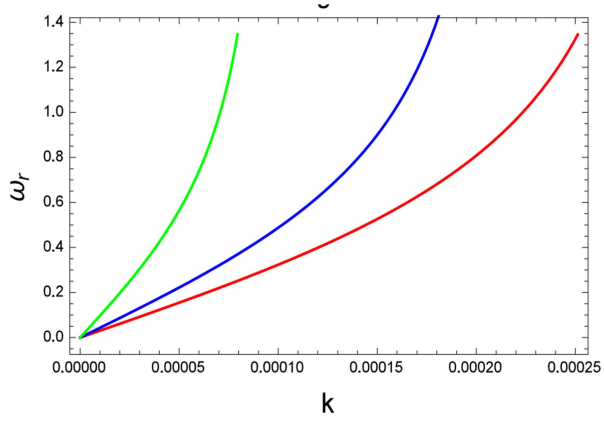

Figure 4: (color online) Showing the variation of ω_r (real part of ω) with k for $n_{c0}= 10^{30}$ cm^{-3}, $n_{r0} = 10^{30}$ cm^{-3}, $n_{e0}= 10^{36}$cm^{-3}(Red line), $n_{e0}= 5 \times 10^{35}$ cm^{-3}(Blue line), $n_{e0}= 10^{35}$ cm^{-3}(Green line), $m_c= 12m_p$, and $m_r= 85m_p$.

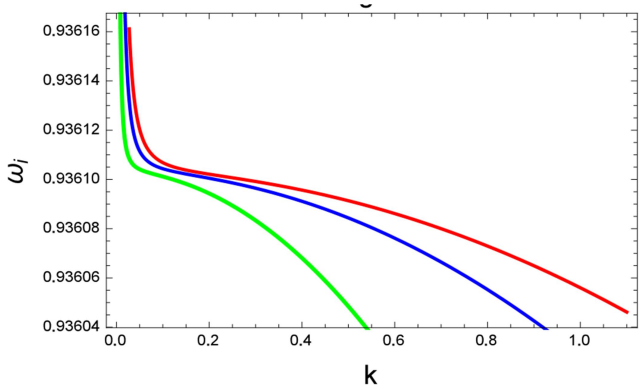

Figure 5: (Color online) Showing the variation of ω_i (imaginary part of ω) with k for $n_{c0}= 10^{30}$ cm^{-3}, $n_{r0}= 10^{30}$ cm^{-3}, $n_{e0}= 10^{36}$ cm^{-3}(Red line), $n_{e0}= 5 \times 10^{35}$ cm^{-3}(Blue line), $n_{e0}= 10^{35}$ cm^{-3}(Green line), $m_e = 9.1 \times 10^{-28}$, $m_c= 12m_p$, and $m_r= 85m_p$.

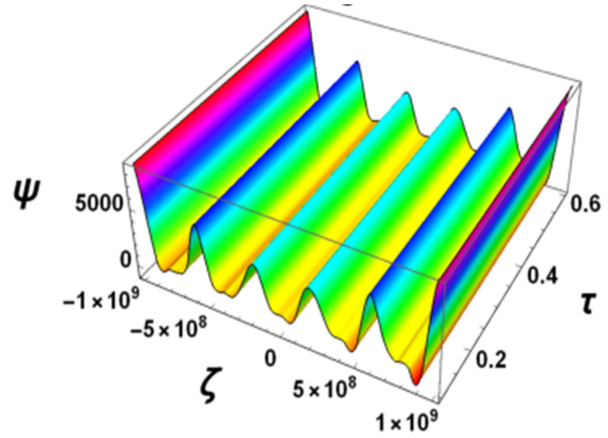

Figure 6: (Color online) showing the time-varying SGPS illustrated by solving Equation (15) numerically. The other parameters are fixed at $v = 0$, $u_0 = 0.05$, $n_{e0}= 10^{36}$ cm^{-3}, $n_{c0}= 10^{30}$ cm^{-3}, $n_{r0}= 10^{30}$ cm^{-3}, $m_c = 12m_p$, and $m_r= 85m_p$.

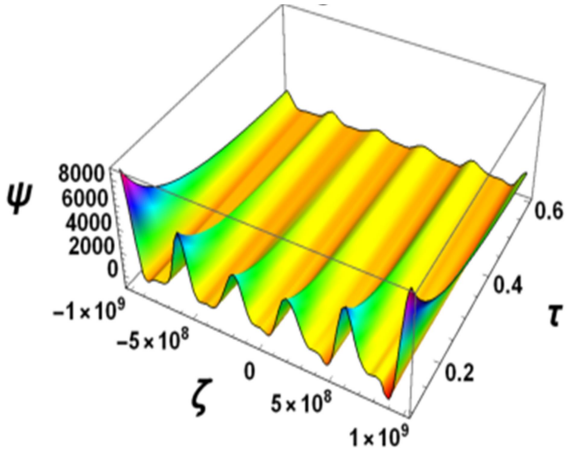

Figure 7: (Color online) Showing the time-varying SGPS in spherical geometry ($v = 2$) illustrated by solving Equation (15) numerically. The other parameters are fixed at $u_0= 0.05$, $m_c= 12\ m_p$, $m_r= 85\ m_p$, $n_{c0}= 10^{30}$cm^{-3}, $n_{r0}= 10^{30}$ cm^{-3},and $n_{e0}= 10^{36}$ cm^{-3}.

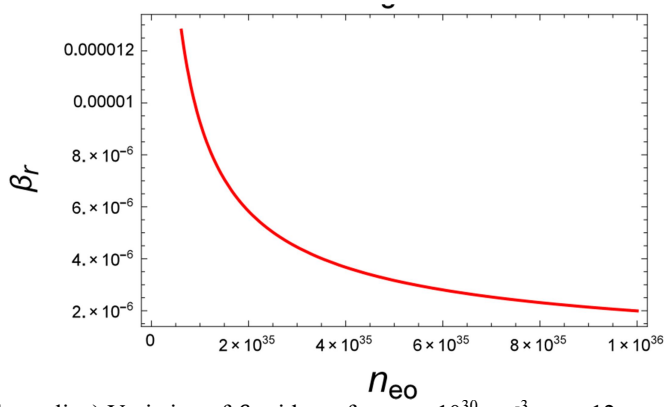

Figure 8: (color online) Variation of β_r with n_{e0} for n_{r0}= 10^{30} cm^{-3}, m_c= $12m_p$, and m_r= $85m_p$.

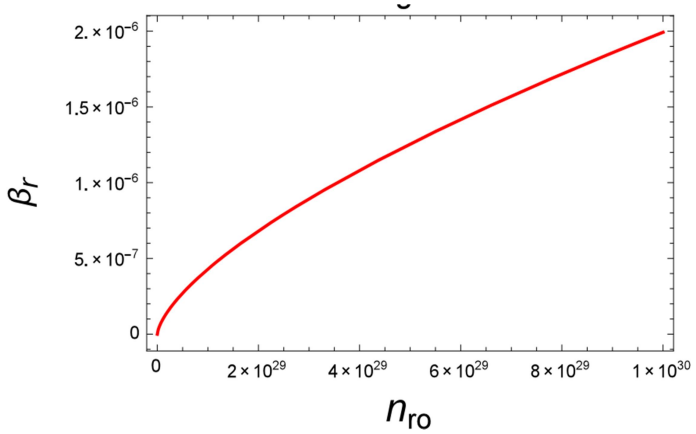

Figure 9: (color online) Variation of β_r with n_{r0} for n_{e0}= 10^{36} cm^{-3}, m_c= $12m_p$, and m_r= $85m_p$.

Now, we want to give our attention to Equation (15) with the term $(\nu/2\tau)\psi_1$(where $\nu = 2$ indicates spherical geometry). We have solved Equation (15) numerically and have also examined the impact of spherical geometry on time-dependent SGPS in the plasma system under consideration. The results are displayed in Figure 7. In our numerical analysis, the initial condition is in the form of the stationary solution of Equation (15) without the term$(\nu/2\tau)\psi_1$, i.e., in the form $\psi_1 = \psi_m Sec^2[\zeta/\Delta]$. Figure 7 discloses the impact of spherical geometry on the fundamental properties of time dependent SGPS in the considered plasma model.

Figure 7 also reveals that the spherical SGPS becomes planar SGPS when τ is large. This is due to the fact that the term relating spherical geometry, $(\nu/2\tau)\psi_1$, becomes non-effective when τ is large. We found that as τdecreases the amplitude of the spherical SGPS increases. The variation of β_r with equilibrium number density of electron and with rubidium number density at equilibrium are shown in Figures 8 and 9, respectively. The variation of β_c with equilibrium number density of electron and carbon number density at equilibrium are also same as Figures 8 and 9, respectively.

6. RESULTS AND DISCUSSION

We have assumed a general non-relativistic DQPS consisting of arbitrary number of light particle species *s* an00.d heavy particle species *j* (both light and heavy particle species are degenerate). We have examined the linear behavior of the SGPM in planar geometry and the non-linear characteristics of this SGPM in both planar and nonplanar (spherical) geometry. The findings of our investigation are reported as follows:

i. The linear SGPM for white dwarf star is unstable when the wavelength is of the order of ~ 10^4 cm.
ii. The position of unstable region changes mainly with the change of the number density of electron and carbon. The frequency versus carbon number density (keeping electron and rubidium number density fixed) curve shows that the position of unstable region shifted as the carbon number density increases and the unstable region is almost independent of *k* when the carbon number density is very low.

iii. The frequency of this mode increases as the electron number density increases and decreases as the carbon number density increases and remains same as the rubidium number density increases or decreases.
iv. As the wavelength of the SGPM increases the positive imaginary part of ω(which is also known as the growth rate) of the SGPM increases almost exponentially while the frequency of the SGPM decreases exponentially.
v. Whenτ decreases the amplitude of the spherical SGPS increases.
vi. The spherical SGPS become planar for higher values of τ.
vii. The spherical SGPS has the larger value of amplitude than the planar SGPS.

We finally stress that our findings will be useful in understanding the basic characteristics of the localized self-gravitational disturbances in neutron stars and white dwarfs which have spherical shape and where the particle number density is of the order of $10^{30}\ cm^{-3}$ or even more.

REFERENCES

Asaduzzaman, M., Mannan A., and Mamun A. A., 2017. Self-gravitational perturbation in super dense degenerate quantum plasmas, Phys. Plasmas. 24, 052102.

Brodin, G. and Marklund M., 2007. Spin magneto-hydrodynamics, New J. Phys. 9, 277.

Chandrasekhar, S., 1931. The density of white dwarf stars, Philos. Mag., 11, 592.

Chandrasekhar, S., 1931a. The maximum mass of ideal white dwarfs, Astrophys. J. 74, 81.

Chandrasekhar, S., 1935. The highly collapsed configurations of a stellar mass (Second paper), Mon. Not. R. Astron. Soc., 170, 405.

Fowler, R. H., 1994. The maxima of absorption lines in stellar spectra (second paper), J. Astrophys. Astr. 15, 241.

Garcia-Berro, E., Torres S., Althaus, L. G., Renedo I., Lorn-Aguiltar P., Crsico A. H., Rohrmann R. D., Salaris M., and Isern J., 2010.A white dwarf cooling age of 8 Gyr for NGC 6791 from physical separation processes, Nature (London), 465, 194.

Haas, F., 2007. Variational approach for the quantum Zakharov system, Phys. Plasmas, 14, 042309.

Hossen, M. A. and Mamun A. A., 2015. Nonlinear ion-acoustic waves in a degenerate plasma with nuclei of heavy elements, Phys. Plasmas, 22, 102710.

Hossen, M. R. and Mamun A. A., 2014. Electrostatic Solitary Structures in Relativistic Degenerate Multispecies Plasma, Braz. J. Phys., 44, 673.

Hossen, M. R., Nahar L., Sultana S., and Mamun A. A., 2014. Nonplanar ion-acoustic shock waves in degenerate plasmas with positively charged heavy ions, High Energy Density Physics 13, 13.

Jeans, J. H., 1929. Astronomy and Cosmology, Cambridge University Press, Cambridge.

Koester, D. and Chanmugam G., 1990. Physics of white dwarf stars, Rep. Prog. Phys. 53, 837.

Marklund, M. and Brodin G., 2007. Dynamics of spin-1/2 quantum plasmas, Phys. Rev. Lett., 98, 025001.

Marklund, M., Eiasson B., and Shukla P. K., 2007. Magnetosonic solutions in a fermionic quantum plasma, Phys. Rev., E 76, 067401.

Masood, W., Eiasson B., and Shukla P. K., 2010. Electromagnetic wave equations for relativistically degenerate quantum magneto plasmas, Phys. Rev., E 81, 066401.

Manfredi, G., 2005. How to model quantum plasmas, Fields Inst. Commun., 46, 263.

Misra, A. P. and Samanta S., 2008. Quantum electron-acoustic double layers in a magneto plasma, Phys. Plasmas 15, 123307.

Misra, A. P., Banerjee S., Haas F., Shukla P. K., and Assis L. P. G., 2010. Temporal dynamics in the one-dimensional quantum Zakharov equations for plasmas, Phys. Plasmas, 17, 032307.

Maxon, S. and Viecelli J., 1974. Spherical Solitons, Phys. Rev. Lett., 32, 4.

Mamun. A. A. and Shukla P. K., 2002. Cylindrical and spherical dust ion-acoustic solitary waves, Phys. Plasmas 9, 1468.

Shapiro, S. L. and Teukolsky S. A., 1983. Black Holes, White Dwarfs, and Neutron Stars: The Physics of Compact Objects, Wiley, New York.

Shukla, P. K. and Eliasson B., 2006. Formation and Dynamics of Dark Solitons and Vortices in Quantum Electron Plasmas, Phys. Rev. Lett., 96, 245001.

Shukla, P. K. and Eliasson B., 2007. Nonlinear Interactions between Electromagnetic Waves and Electron Plasma Oscillations in Quantum Plasmas, Phys. Rev. Lett., 99, 096401.